

Accelerated wound healing by injectable microporous gel scaffolds assembled from annealed building blocks

Donald R. Griffin^{1†}, Westbrook M. Weaver^{2†}, Philip O. Scumpia³, Dino Di Carlo^{4*} and Tatiana Segura^{5*}

Injectable hydrogels can provide a scaffold for *in situ* tissue regrowth and regeneration, yet gel degradation before tissue reformation limits the gels' ability to provide physical support. Here, we show that this shortcoming can be circumvented through an injectable, interconnected microporous gel scaffold assembled from annealed microgel building blocks whose chemical and physical properties can be tailored by microfluidic fabrication. *In vitro*, cells incorporated during scaffold formation proliferated and formed extensive three-dimensional networks within 48 h. *In vivo*, the scaffolds facilitated cell migration that resulted in rapid cutaneous-tissue regeneration and tissue-structure formation within five days. The combination of microporosity and injectability of these annealed gel scaffolds should enable novel routes to tissue regeneration and formation *in vivo*.

The evolution of injectable materials for regenerative medicine has been driven by the need to recapitulate natural tissue function with a minimally invasive implantation procedure^{1–3}. Optimization of these materials has been focused on tuning their bulk properties to regulate cell behaviour through material stiffness⁴ and chemical moieties, such as oligopeptides and growth factors^{2,5}. Ultimately, these approaches are limited by physical constraints, as host cells must remodel this precisely tuned matrix to infiltrate and fully integrate with the material.

Successful materials for tissue regeneration must precisely match the rate of material degradation to tissue development. If degradation occurs too quickly then insufficient scaffolding will remain to support tissue ingrowth, whereas a rate that is too slow will prevent proper tissue development and can promote fibrosis⁶. Tuning of degradation rates based on local environment has been approached using hydrolytically and enzymatically degradable materials^{7,8}; however, decoupling cellular infiltration with decreases in material mechanical stability has proved extremely challenging¹. Promotion of cellular infiltration into the material can be approached using a lightly crosslinked matrix; however, this often results in mechanical mismatch with surrounding tissues and poor material stability⁹. Alternatively, the hydrogel degradation rate can be tuned by altering the polymeric backbone identity¹⁰ or crosslinking density¹¹, matching the rates of degradation and tissue formation. Although these techniques address specific limitations of injectable hydrogels, they do not provide a robust pathway to achieve bulk tissue integration that does not rely on prior material degradation.

Every wound site is unique in its physical and chemical requirements for functional tissue regeneration, requiring a material

strategy that is robust to a variety of challenging degradation environments. We have created a new class of injectable biomaterials—microporous annealed particle (MAP) gels—that circumvent the need for material degradation before tissue ingrowth by providing a stably linked interconnected network of micropores for cell migration and bulk integration with surrounding tissue. Inspired by the success of microporous scaffolds generated *ex situ* (through the use of porogens^{12–15}) that promote cell migration, we designed an injectable biomaterial that also possesses these interconnected networks by using a porogen-free, building-block approach to scaffold formation. Our strategy to achieve these favourable features relies on the self-assembly of highly monodisperse hydrogel microparticle (microgel) building blocks formed by microfluidic water-in-oil droplet segmentation^{16–18} (Fig. 1a). Lattices of microgel building blocks are then annealed to one another via surface functionalities to form an interconnected microporous scaffold either with or without cells present in the interconnected pores (Fig. 1b,c). Microparticles have been used successfully for cellular encapsulation¹⁹ and assembly^{20,21} *in vitro*, as well as neural cell-coated delivery vehicles *in vivo*^{22,23}; however, they have not been explored as covalently linked three-dimensional scaffolding for tissue regeneration. Further, the MAP scaffold can be injected and moulded to any shape (Fig. 1d), providing a mechanically stable scaffold of interconnected microporous networks for cell ingrowth (Fig. 1e).

By combining injectability and microporosity, we have provided a unique biomaterial scaffold for efficient cellular network formation *in vitro* and bulk tissue integration *in vivo*. Our modular material also provides mechanical support for rapid cell migration, molecular cues to direct cell adhesion, and resorption after tissue regeneration.

¹Department of Chemical and Biomolecular Engineering, University of California, Los Angeles, Los Angeles, California 90095, USA. ²Department of Bioengineering, University of California, Los Angeles, Los Angeles, California 90095, USA. ³Division of Dermatology, David Geffen School of Medicine, University of California, Los Angeles, Los Angeles, California 90095, USA. ⁴Department of Bioengineering, California NanoSystems Institute, Jonsson Comprehensive Cancer Center, University of California, Los Angeles, Los Angeles, California 90095, USA. ⁵Department of Chemical and Biomolecular Engineering, California NanoSystems Institute, Jonsson Comprehensive Cancer Center, University of California, Los Angeles, Los Angeles, California 90095, USA. †These authors contributed equally to this work. *e-mail: dicarlo@ucla.edu; tsegura@ucla.edu

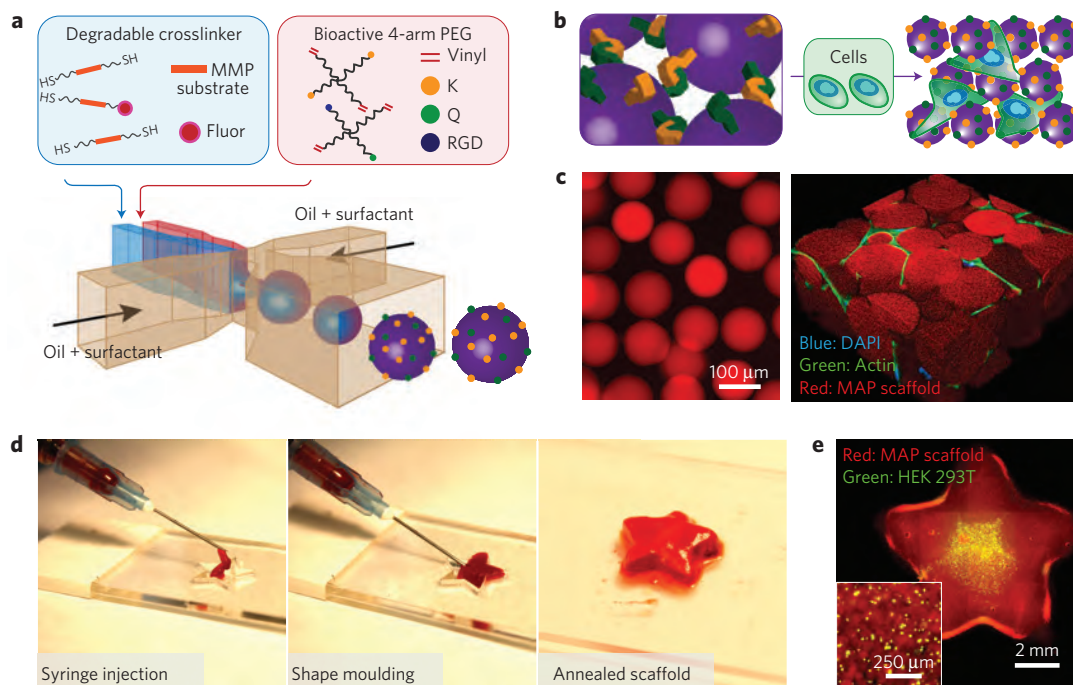


Figure 1 | Microfluidic generation of microsphere hydrogel building blocks for the creation of microporous annealed particle (MAP) scaffolds. **a**, Scheme illustrating microgel formation using a microfluidic water-in-oil emulsion system. A pre-gel and crosslinker solution are segmented into monodisperse droplets followed by in-droplet mixing and crosslinking via Michael addition. **b**, microgels are purified into an aqueous solution and annealed using FXIIIa into a microporous scaffold, either in the presence of cells or as a pure scaffold. **c**, Fluorescent images showing purified microgel building blocks (left) and a subsequent cell-laden MAP scaffold (right). **d**, MAP scaffolds are mouldable to macroscale shapes, and can be injected to form complex shapes that are maintained after annealing. **e**, This process can be performed in the presence of live cells.

Through microfluidic fabrication, we precisely tailor the chemical and physical properties of the building blocks, allowing downstream control of the properties of the emergent MAP scaffolds. Our novel building-block-based approach, in which robustly achieved imperfect self-assembly is desirable to achieve microporosity, fundamentally changes the use and implementation of injectable hydrogels as tissue mimetic constructs for bulk tissue integration.

From building blocks to porous scaffolds

We used a microfluidic water-in-oil emulsion approach^{16–18} to segment a continuous pre-gel aqueous phase into uniform scaffold building blocks¹⁹ (Fig. 1a and Supplementary Fig. 1a–c). Generating microgel building blocks serially at the microscale, rather than using the typical vortex and sonication-based approaches^{24,25}, allowed tight control over the formation environment and ultimate material properties of the emergent MAP gel. By tuning the flow rates of both the pre-gel solution and the pinching oil flow, as well as the geometry of the microfluidic channel, we created a range of microgel sizes with low polydispersity (Fig. 2a–c). Although our fabrication method was serial, it retained practicality in its high-throughput nature, with generation rates that ranged from 250 Hz for larger particles (>100 μm) to ~1,200 Hz for small particles (~15 μm). This translated to roughly 100 μl of pre-swollen gel every 50 min for a single device. This approach ultimately resulted in particles that were highly monodisperse, both physically and chemically. Microfluidic generation of MAP building blocks is a readily scalable process: a practical requirement for wide adoption and use²⁶.

The resultant microgel building blocks were composed of a completely synthetic hydrogel mesh of multi-armed poly(ethylene) glycol–vinyl sulphone (PEG–VS) backbones decorated with cell-adhesive peptide (RGD) and two previously used transglutaminase peptide substrates^{27–29} (K and Q). The microgels were crosslinked via Michael-type addition with cysteine-terminated matrix

metalloprotease-sensitive peptide sequences that allowed cell-controlled material degradation and subsequent resorption. The microgel building blocks were purified into an aqueous solution of isotonic cell culture media for storage.

The microgel building blocks were annealed to one another to form a MAP gel via a non-canonical amide linkage between the K and Q peptides mediated by activated Factor XIII (FXIIIa), a naturally occurring enzyme responsible for stabilizing blood clots²⁸. This enzyme-mediated annealing process allowed incorporation of living cells into a dynamically forming MAP scaffold that contained interconnected microporous networks. Following addition of FXIIIa, but before scaffold annealing, a slurry of the microgel building blocks can be delivered via syringe application, ultimately solidifying in the shape of the cavity into which they are injected (Fig. 1d,e). Structural changes leading to over a threefold increase in storage modulus in the annealed gels was observed on addition of FXIIIa to the microgel building blocks (Fig. 2d). We confirmed microgel annealing was necessary for scaffold formation via high-vacuum SEM observation, wherein on dehydration the scaffolds adopted a highly stretched but interconnected mesh, whereas building blocks without FXIIIa separated into individual spherical beads (Supplementary Fig. 2d,e).

By tuning the microgel building-block size and composition we were able to generate a diverse set of assembled MAP scaffolds. By using building-block sizes from 30 to 150 μm in diameter, we achieved networks with median pore diameters ranging from ~10 to ~35 μm (Fig. 2e,f). We also screened different PEG weight percentages and crosslinker stoichiometries to demonstrate a range of easily achievable building-block storage moduli from ~10 to 1,000 Pa (Supplementary Fig. 2a–c), which spans the stiffness regime necessary for mammalian soft tissue mimetics^{30–34}. Physically matched MAP and non-porous gels demonstrated differential degradation

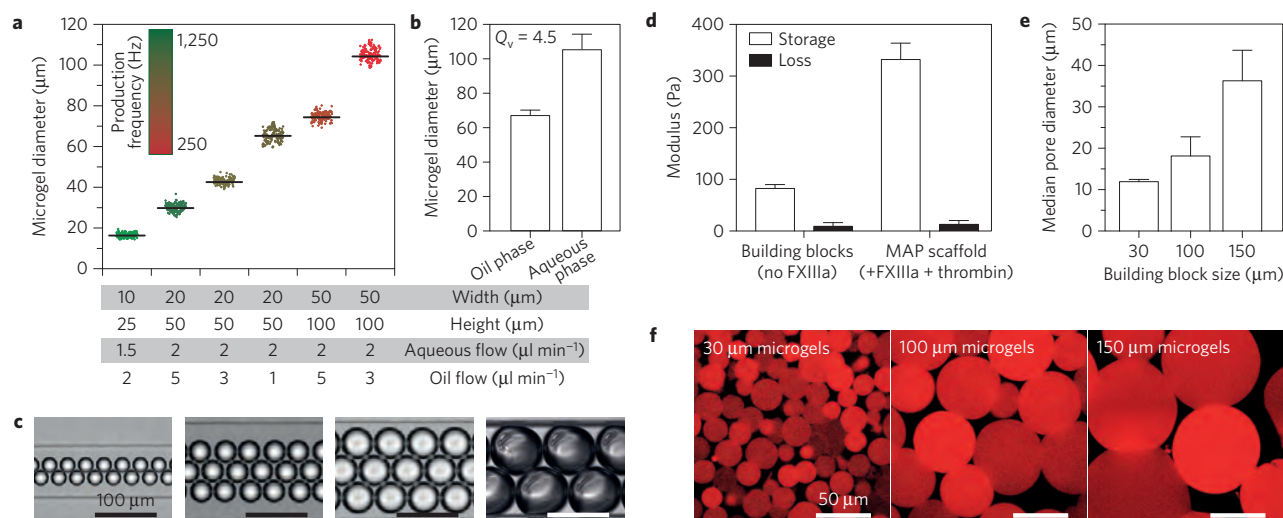


Figure 2 | High-precision fabrication of microgel building blocks allows the creation of defined MAP scaffolds. **a**, The operational regime for microfluidic microgel generation has a large dynamic range, spanning almost an order of magnitude in size while maintaining tight control at each condition, with CVs < 6% in all cases. **b**, Hydrogel building blocks swell in buffer after aqueous extraction from the oil phase. The swelling ratio (Q_v) is predictable and determined by polymer network characteristics. In our chosen formulation, $Q_v = 4.5$. **c**, Representative images of microgel droplets in flow after generation. **d**, Rheological characterization of the MAP scaffold. Without the addition of FXIIIa the microgel building blocks exhibit some gel-like characteristics; however, the onset of annealing results in significantly increased macroscale mechanical moduli. **e**, Different building-block sizes allow deterministic control over resultant microporous network characteristics, presented here as median pore sizes \pm s.d. **f**, Single confocal slices of MAP scaffolds created using different building-block sizes. All data presented as average \pm s.d. unless otherwise stated. All experiments performed in triplicate.

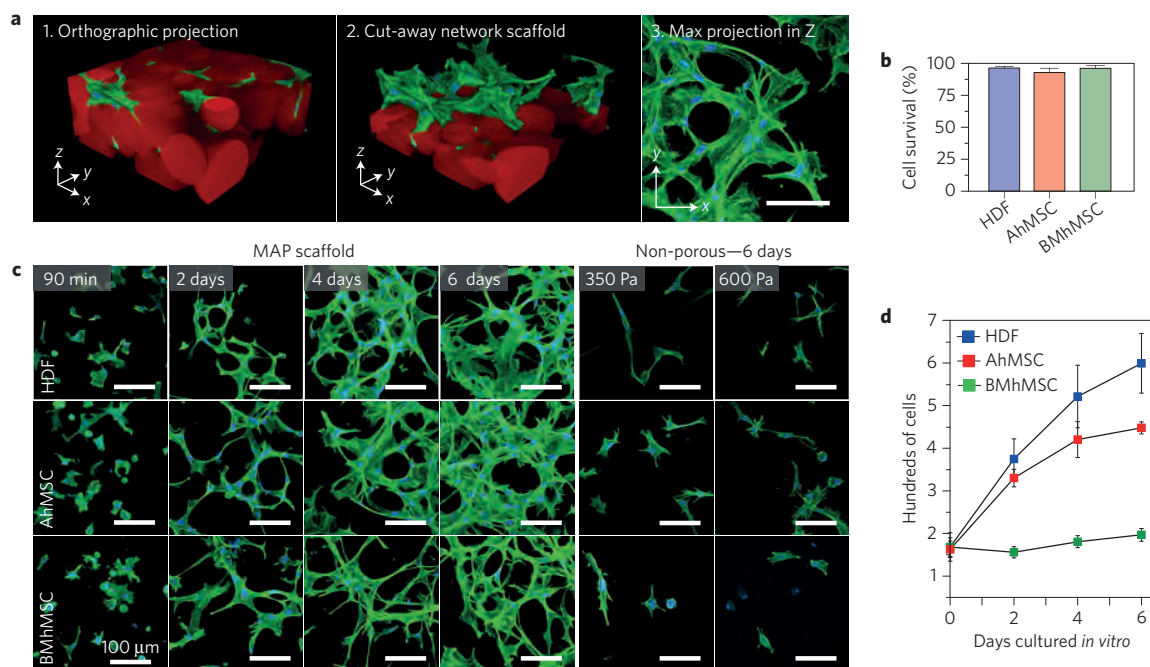


Figure 3 | MAP scaffolds facilitate 3D cellular network formation and proliferation *in vitro*. **a**, Schematic illustrating how to read images of 3D cell growth and network formation presented in **c**. **b**, Cell survival 24 h post annealing is greater than 93% across three cell lines representing different human tissue types. HDF, human dermal fibroblasts; AhMSC, adipose-derived human mesenchymal stem cells; BMhMSC, bone marrow-derived human mesenchymal stem cells. **c**, Fluorescent images demonstrating the formation of 3D cellular networks during six days of culture in MAP scaffolds *in vitro* as well as non-porous gels after six days. (350 Pa, bulk modulus identical to MAP; 600 Pa, microscale modulus matched to individual microgels). **d**, Cells proliferate within the MAP scaffold while forming interconnected networks. HDF and AhMSC cells proliferate quickly within the scaffolds, with doubling times of ~ 1.5 and ~ 2 days, respectively. BMhMSC cells proliferate significantly more slowly, with a calculated doubling time of ~ 12 days. These are analogous to previously observed normal growth phenotypes for these lines. All data presented as average \pm s.d. All experiments performed in triplicate.

kinetics when exposed to a protease cocktail *in vitro*, indicating greater access of the protease to MMP-cleavable sites within the MAP gel due to its microscale porosity (Supplementary Fig. 2D).

Proliferation and 3D network formation *in vitro*

To assess the ability of the MAP scaffold to support cell growth and network formation, we developed an *in vitro* cell morphology and

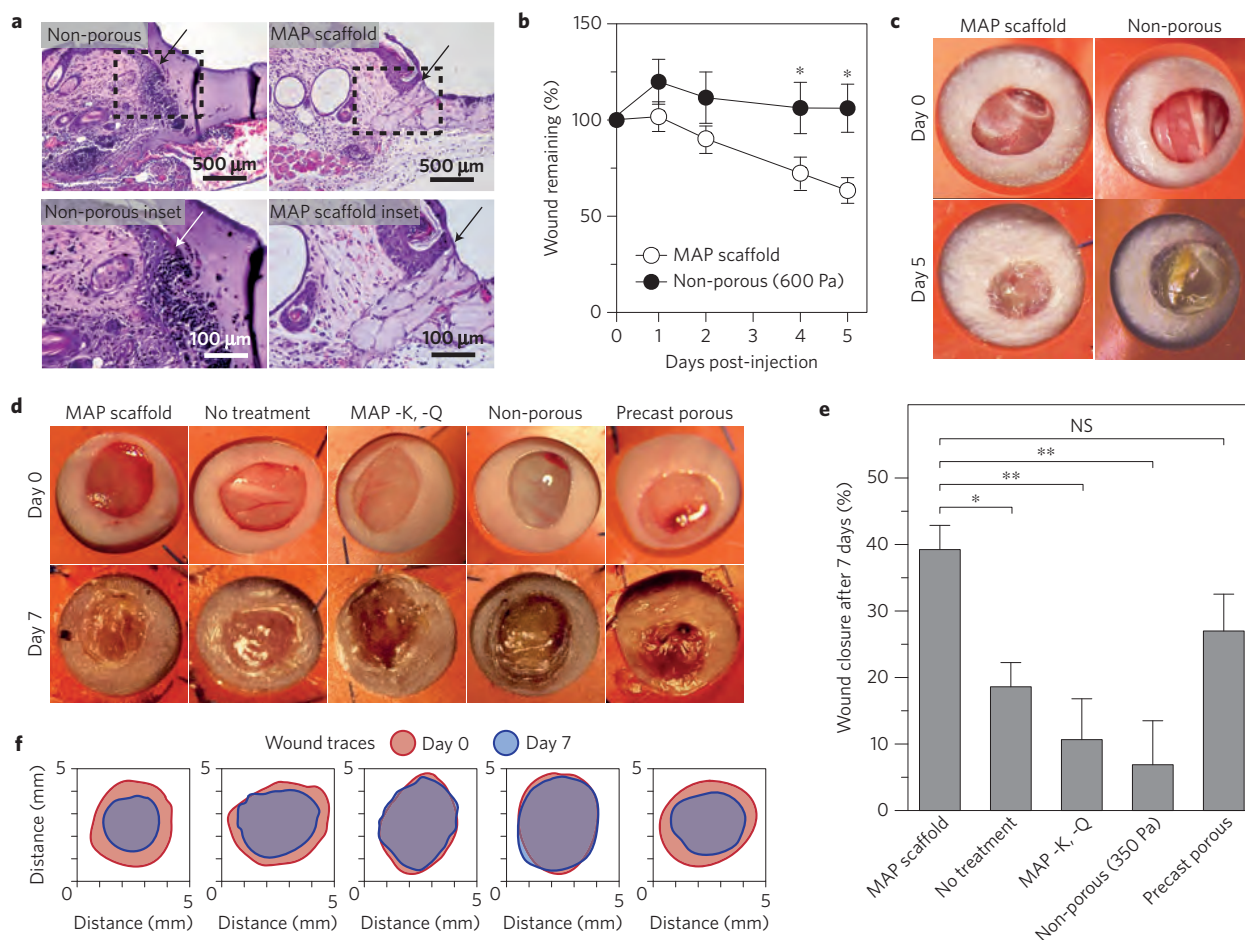


Figure 4 | MAP scaffolds promote fast wound closure in SKH1-Hr^{Hr} and Balb/c epidermal mouse models. **a**, H&E staining of tissue sections indicate seamless integration of the injected MAP scaffold as well as the non-porous control 24 h post injection in SKH1-Hr^{Hr} mice. **b**, Quantification of wound closure over a five-day period shows statistically significant wound-closure rates for MAP scaffolds when compared with non-porous bilateral controls ($N=6$). Statistical significance performed using standard two-tailed t -test ($*p < 0.05$). **c**, Representative images of wound closure during a five-day *in vivo* wound-healing model in SKH1-Hr^{Hr} mice. **d**, Representative images of wound closure during seven-day *in vivo* Balb/c experiments. **e**, Quantification of wound-closure data from Balb/c *in vivo* wound healing. After seven days *in vivo*, the MAP scaffolds promote significantly faster wound healing than the no-treatment control, the non-porous PEG gel, and the MAP gels lacking the K and Q peptides. Porous gels created *ex vivo* to precisely match the wound shape using the canonical, porogen-based, casting method showed appreciable wound-healing rates, comparable to the MAP scaffolds, but lacking injectability ($N=5-7$). **f**, Traces of wound-bed closure during seven days *in vivo* for each treatment category. All data are presented as average \pm s.e.m. Statistical significance performed using one-way ANOVA with a Dunnett *post hoc* multiple comparison test ($*p < 0.05$; $**p < 0.01$).

proliferation model using three human cell lines: dermal fibroblasts (HDF), adipose-derived mesenchymal stem cells (AhMSC), and bone marrow-derived mesenchymal stem cells (BMhMSC). We dynamically incorporated a single-cell suspension within a FXIIIa-annealed MAP gel. The three cell lines exhibited high cell viability ($\geq 93\%$, Fig. 3b) following 24 h of culture within the MAP scaffold. The HDF and AhMSC cell lines demonstrated continued proliferation over a six-day culture period, with doubling times of 1.5 and 2 days, respectively (Fig. 3d). BMhMSCs were observed to undergo proliferation as well—however, with an extended calculated doubling time of ~ 12 days.

Cells incorporated into the MAP scaffold began to exhibit spread morphology 90 min following the onset of annealing (Fig. 3c and Supplementary Figs 3 and 4). After two days in culture, all observed cells within the MAP scaffolds exhibited a completely spread morphology, which continued through day 6. Importantly, we observed extensive network formation for all cell lines by day 2. Cell networks increased in size and complexity through the entirety of the experiment. The BMhMSCs were of particular note, as their expansive network formation and

slower proliferation rate indicated that these cells were able to spread to extreme lengths, forming highly interconnected cellular networks within the microporous scaffolds. Notably, cells that were grown in non-porous gels of identical chemical properties (5 wt%, $G' = 600$ Pa gel, Fig. 3c) or mechanical properties (4.5 wt%, $G' = 350$ Pa gel, Fig. 3c) maintained viability, but did not exhibit any appreciable network formation, even after six days in culture (Supplementary Fig. 4).

Seamless integration and normal tissue architecture *in vivo*

We hypothesized that the ability of the MAP scaffolds to enable both cell proliferation and expedient network formation *in vitro* was indicative of an ability to support *in vivo* cell migration and bulk tissue integration within the scaffold. To test our hypothesis, we used a murine skin wound-healing model³⁵, addressing a tissue of interest for previous implanted porous biomaterials³⁶⁻³⁸. Wound contraction, critical for skin healing in loose-skinned mammals (including mice), was prevented using a sutured rubber splint. This technique allows healing through re-epithelialization and granulation, better simulating the healing response of humans and

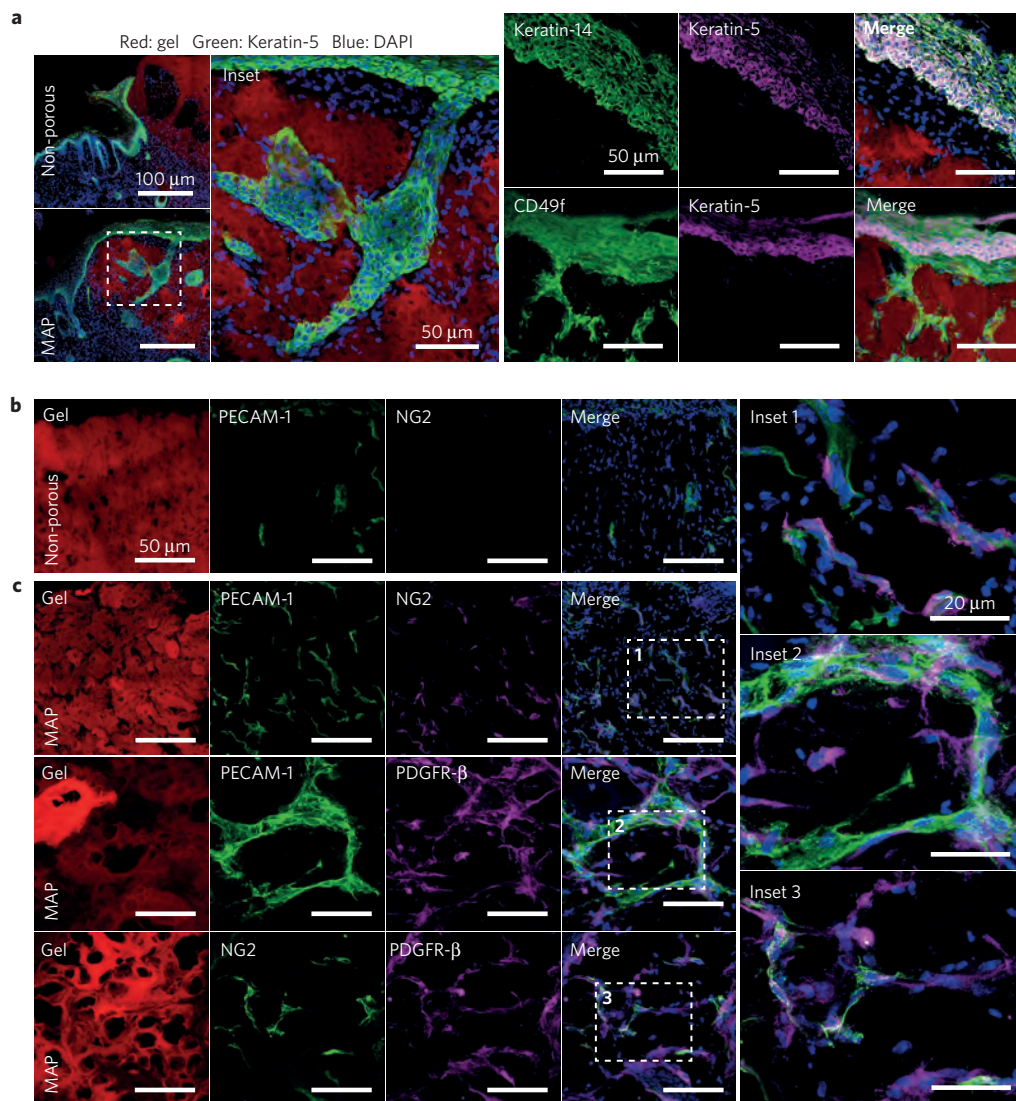


Figure 5 | MAP scaffolds allow faster tissue regeneration compared with non-porous controls *in vivo*. **a**, Matching wound-closure data (Fig. 4), the MAP scaffolds also allow significant re-epithelialization five days post injection. By comparison, the non-porous constructs show very little to no re-epithelialization by day 5. Importantly, in addition to stratified expression of keratin-5, keratin-14 and CD49f above the gel, we also observe large-scale tissue structures within the construct. Keratin-5 staining of the basement epithelial layer outline developing hair follicles and sebaceous glands within the MAP scaffold after five days. Non-porous controls are devoid of similar complex multicellular structures. **b**, Non-porous gels show some PECAM-1 positive cells ingrowth, however, there is no positive staining for supporting vascular cells (NG2). **c**, MAP scaffolds contain large networks of cells staining positive for the endothelial marker, PECAM-1, juxtapositioned with cells expressing NG2 and PDGFR- β (a pericyte phenotype), indicative of developing vasculature.

fixed-skinned mammals^{35,39}. Because of the injectability of the MAP scaffold, we were able to deliver the microgel building blocks directly to the wound site, followed by *in situ* annealing via exogenous FXIIIa (activated in the wound bed by exogenous thrombin). This provided a seamless interface by simultaneously linking MAP building blocks to one another as well as to endogenous lysine and glutamine residues present in the surrounding tissue (Fig. 4a, right). Similarly, a seamless interface was observed for the chemically identical, non-porous bilateral control (Fig. 4a, left). Despite their similar interface, the MAP scaffold resulted in significantly faster wound closure than the non-porous controls (60% versus 100% remaining wound area after five days, respectively) when injected into the wounds of hairless (CLR:SKH1-*Hr^{hr}*) mice (Fig. 4b,c).

Accelerated wound closure mediated by the MAP scaffold was also observed in a longer wound-healing experiment performed in BALB/c mice. After seven days *in vivo*, the MAP scaffold led to 39%

wound closure, significantly greater than the no-treatment control, which allowed only 19%, and the physically matched non-porous control, which allowed 7%. Non-annealing microgels, which lacked K and Q peptides, were unable to facilitate increased wound closure (only 10%) compared to the no-treatment control. This indicates that the annealing process is critical to support faster wound closure, which is not due to the presence of microgels in the wound bed alone. Microporous gels created using a porogen-based casting method also showed an increased wound healing (27%) compared with a no-treatment control, further supporting the hypothesis that microscale porosity enhances wound healing *in vivo*.

The disparities in wound-closure rates led us to investigate the differences in tissue responses to the non-porous and MAP injectable gel. MAP scaffold injection resulted in extensive wound re-epithelialization after five days *in vivo*. We observed keratin-5⁺ cells with stratified squamous morphology (Fig. 5a, bottom panel, green) over the surface of the MAP scaffold; however, no cells (keratin-5⁺

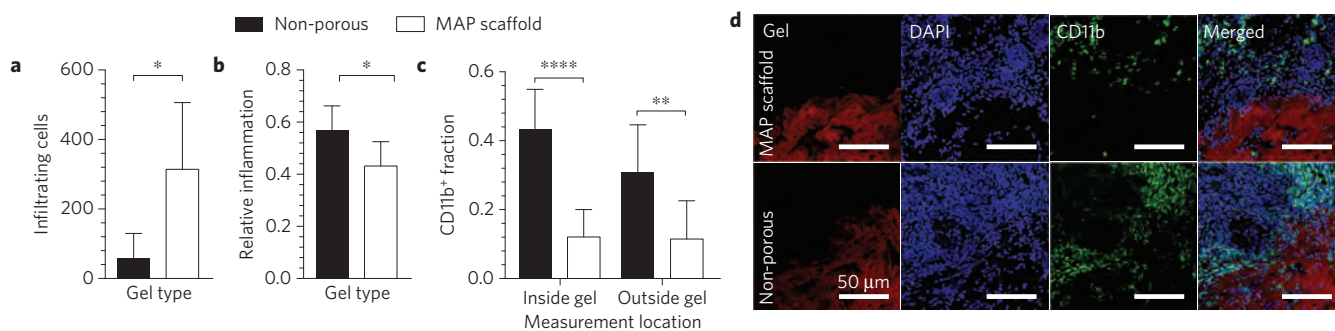


Figure 6 | MAP scaffolds elicit a significantly lower immune response than non-porous hydrogels *in vivo*. **a,b**, Quantification of total cellular infiltration into the constructs (**a**) and immune response in the surrounding tissue 24 h post injection (**b**). Inflammation is measured using a paired test for each mouse, where the fraction is the number of inflammatory cells for each construct relative to its bilateral control. **c**, Quantification of immune response five days after injection, as measured by the fraction of total cells expressing CD11b. MAP scaffolds elicit a significantly lower response of CD11b⁺ cells as compared with non-porous controls, both inside the construct and in the surrounding tissue ($N=6$ for **a-c**). **d**, Representative images of tissue sections from five days after injection for MAP scaffolds and non-porous controls. All data presented as average \pm s.d. Statistical significance performed using standard two-tailed *t*-test (* $p < 0.05$; ** $p < 0.01$; **** $p < 0.001$).

or otherwise) were observed past the non-porous wound edge (Fig. 5a, top panel, green). Importantly, the MAP scaffold was able to sustain the formation of what appeared to be a developing hair follicle with adjoining sebaceous gland within the wound bed (Fig. 5a, inset) resembling the structure of these glands in the uninjured skin (Supplementary Fig. 7). Further, we observed other instances of large keratin-5⁺ tissue structures within the MAP scaffold, including tubular structures and epithelial invaginations (Supplementary Fig. 7). Expression of the epithelial markers keratin-5, keratin-14 and CD49f was observed in both normal epidermis (Supplementary Fig. 8) and the keratinocytes and newly formed basement membrane of the regenerating epidermis overlying the MAP gel. As expected, staining of keratin-5 and -14 in the regenerating epidermis extended beyond the basilar keratinocytes, as shown by the expansion of staining beyond the basilar layer and into the stratifying epidermis, consistent with a hyperproliferative epidermis⁴⁰ (Fig. 5a, right panels). These data indicate normal epithelial regeneration over the wound beds treated with MAP gel. Although beyond the scope of this manuscript, we hypothesize that, together, these results are an indication of higher-order collective migration (that is, movement of multicellular clusters in concert) contributing to epidermal regeneration. Although cells were able to infiltrate the non-porous bilateral controls (as indicated by DAPI staining), no evidence of re-epithelialization or cutaneous-tissue formation was found after five days *in vivo*.

Through further investigation, we found that the MAP scaffold promoted bulk integration via complex vascular network formation *in vivo*^{41–44}. After five days, both endothelial cells (PECAM-1⁺) and supporting pericytes (both NG2⁺ and PDGFR β ⁺; refs 45,46; Fig. 5c) were present within the MAP scaffold, whereas only single branches of endothelial cells without supporting pericytes were present in the non-porous bilateral controls (Fig. 5b). The presence of co-localized endothelial cells and pericytes was evidence of a developing vascular network⁴⁷. To our knowledge, this is the first instance of early (<7 days) pericyte migration into a synthetic injectable material or implanted porous scaffold without the inclusion of exogenous growth factors^{36,37,48,49}.

While investigating the seamless interface provided by the injectable scaffolds, we observed differences in both overall and immune cell quantities at day 1 within an area extending 75 μ m into the scaffold and 75 μ m into the tissue adjacent to the scaffold (Supplementary Fig. 6). H&E staining revealed that one day post injection, the MAP scaffolds contained significantly higher numbers of leukocytes within the scaffold, whereas the non-porous bilateral controls exhibited aggregation of leukocytes at the skin

edge near the interface of the wound and scaffold (Fig. 6a). This corroborated the greater ease of cell mobility previously observed in our *in vitro* network formation experiments (Fig. 3). Further, the MAP scaffold and its surrounding tissue contained a significantly lower number of leukocytes (determined by a dermatopathologist blinded to the identity of the experimental treatment using standard H&E) when compared with the non-porous bilateral control of the same mouse (Fig. 6b). Consistent with one-day-old wounds, greater than 90% of the leukocytes infiltrating the skin tissue or the MAP scaffold were neutrophils, as evidenced by their polymorphonuclear characteristic and granular cytoplasm. These results indicated a lower apparent inflammatory response to the MAP scaffolds at day 1, and are consistent with previous studies demonstrating that porous scaffolds allow better infiltration of inflammatory cells, whereas non-porous scaffolds result in a barrier to tissue healing and accumulation of inflammatory cells at the wound/scaffold interface^{50,51}. After five days post injection, lower fractions of cells staining positive for CD11b (a marker for cells of the myeloid lineage responsible for early tissue inflammation^{52,53}) were present both in the surrounding tissue and within the MAP scaffold relative to the non-porous controls (Fig. 6c,d), suggesting a sustained lower inflammatory response⁵⁴ and in agreement with what has been observed in other microporous scaffolds that are cast *ex vivo* and implanted *in vivo*¹². Combined, these results support an at present underexplored geometric component to immune stimulation from chemically identical injectable biomaterials.

MAP scaffolds as a modular biomaterial

MAP scaffolds represent a new class of injectable biomaterial that introduces microscale interconnected porosity through robustly achieved imperfect self-assembly and annealing of individual building blocks. This general approach has potential to address both clinical and *in vitro* needs for improved biomaterials. The ability of a MAP scaffold to completely fill tissue voids while providing interconnected microporosity could transform clinical wound treatment by acting as a mouldable skin substitute, and as a synthetic alternative to grafting technology. Further, the injectable nature of the scaffold allows it to be applied to any wound size and shape. This is an important characteristic when considering internal wound-healing and regeneration applications for functional tissues.

For *in vitro* use, FXIIIa-mediated annealing allows incorporation of living cells into the scaffold as it is assembled, useful for the creation of three-dimensional supported cellular structures. Using sets of different building blocks, these structures can possess spatial complexity and should develop multicellular connectivity

on timescales previously unobtainable using current assembly techniques^{20,21}. MAP gels also have advantages in terms of more rapid invasion and cellular level connectivity over gels at present available (for example, Matrigel) for 3D cell culture *in vitro*, and could be a critical enabler of organ-on-a-chip technologies.

We present a fundamental change in the approach to bottom-up modular biomaterials by using the negative space of lattice formation to promote the development of complex three-dimensional networks on timescales previously unseen using current hydrogel technologies. The 'plug and play' nature of this microfluidically generated building-block strategy allows the incorporation of a wide range of already established materials (for example, fibrin or hyaluronic acid), signals (for example, growth factors) and cell populations (for example, stem cells). Complex combinations of building blocks with deterministic chemical and physical properties may enable tissue regeneration in a range of distinct physiological niches (for example, neural, cardiac, skin, and so on), where MAP scaffolds are tailored to each niche via their building-block properties. The unique combination of microporosity, injectability and modular assembly inherent to MAP scaffolds has the potential to alter the landscape of tissue regeneration *in vivo* and tissue creation *de novo*.

Received 20 November 2014; accepted 15 April 2015;

published online 1 June 2015

References

- Lee, K. & Hubbell, J. A. Tissue, cell and engineering. *Curr. Opin. Biotechnol.* **24**, 827–829 (2013).
- Guvendiren, M. & Burdick, J. A. Engineering synthetic hydrogel microenvironments to instruct stem cells. *Curr. Opin. Biotechnol.* **24**, 841–846 (2013).
- Discher, D. E., Mooney, D. J. & Zandstra, P. W. Growth factors, matrices, and forces combine and control stem cells. *Science* **324**, 1673–1677 (2009).
- Huebsch, N. *et al.* Harnessing traction-mediated manipulation of the cell/matrix interface to control stem-cell fate. *Nature Mater.* **9**, 518–526 (2010).
- Wade, R. J. & Burdick, J. A. Engineering ECM signals into biomaterials. *Mater. Today* **15**, 454–459 (October, 2012).
- Alijotas-Reig, J., Fernández-Figueras, M. T. & Puig, L. Late-onset inflammatory adverse reactions related to soft tissue filler injections. *Clin. Rev. Allergy Immunol.* **45**, 97–108 (2013).
- Lutolf, M. P. *et al.* Synthetic matrix metalloproteinase-sensitive hydrogels for the conduction of tissue regeneration: Engineering cell-invasion characteristics. *Proc. Natl Acad. Sci. USA* **100**, 5413–5418 (2003).
- Galler, K. M., Aulisa, L., Regan, K. R., D'Souza, R. N. & Hartgerink, J. D. Self-assembling multidomain peptide hydrogels: Designed susceptibility to enzymatic cleavage allows enhanced cell migration and spreading. *J. Am. Chem. Soc.* **132**, 3217–3223 (2010).
- Wang, D.-A. *et al.* Multifunctional chondroitin sulphate for cartilage tissue–biomaterial integration. *Nature Mater.* **6**, 385–392 (2007).
- Kong, H. J., Kaigler, D., Kim, K. & Mooney, D. J. Controlling rigidity and degradation of alginate hydrogels via molecular weight distribution. *Biomacromolecules* **5**, 1720–1727 (2004).
- Burdick, J. A., Chung, C., Jia, X., Randolph, M. A. & Langer, R. Controlled degradation and mechanical behavior of photopolymerized hyaluronic acid networks. *Biomacromolecules* **6**, 386–391 (2005).
- Madden, L. R. *et al.* Proangiogenic scaffolds as functional templates for cardiac tissue engineering. *Proc. Natl Acad. Sci. USA* **107**, 15211–15216 (2010).
- Stachowiak, A. N., Bershteyn, A., Tzatzalos, E. & Irvine, D. J. Bioactive hydrogels with an ordered cellular structure combine interconnected macroporosity and robust mechanical properties. *Adv. Mater.* **17**, 399–403 (2005).
- Gorgieva, S. & Kokol, V. Preparation, characterization, and *in vitro* enzymatic degradation of chitosan-gelatin hydrogel scaffolds as potential biomaterials. *J. Biomed. Mater. Res. A* **100**, 1655–1667 (2012).
- Sokic, S., Christenson, M., Larson, J. & Papavasiliou, G. *In situ* generation of cell-laden porous MMP-sensitive PEGDA hydrogels by gelatin leaching. *Macromol. Biosci.* **14**, 731–739 (2014).
- Hosokawa, K., Fujii, T. & Endo, I. Handling of picoliter liquid samples in a poly(dimethylsiloxane)-based microfluidic device. *Anal. Chem.* **71**, 4781–4785 (1999).
- Anna, S. L., Bontoux, N. & Stone, H. A. Formation of dispersions using 'flow focusing' in microchannels. *Appl. Phys. Lett.* **82**, 364–366 (2003).
- Kawakatsu, T., Kikuchi, Y. & Nakajima, M. Regular-sized cell creation in microchannel emulsification by visual microprocessing method. *J. Am. Oil Chem. Soc.* **74**, 317–321 (1997).
- Li, C. Y., Wood, D. K., Hsu, C. M. & Bhatia, S. N. DNA-templated assembly of droplet-derived PEG microtissues. *Lab Chip* **11**, 2967–2975 (2011).
- Du, Y., Lo, E., Ali, S. & Khademhosseini, A. Directed assembly of cell-laden microgels for fabrication of 3D tissue constructs. *Proc. Natl Acad. Sci. USA* **105**, 9522–9527 (2008).
- Qi, H. *et al.* DNA-directed self-assembly of shape-controlled hydrogels. *Nature Commun.* **4**, 2275 (2013).
- Jgamadze, D. *et al.* Colloids as mobile substrates for the implantation and integration of differentiated neurons into the mammalian brain. *PLoS ONE* **7**, e30293 (2012).
- Pautot, S., Wyart, C. & Isacoff, E. Y. Colloid-guided assembly of oriented 3D neuronal networks. *Nature Methods* **5**, 735–740 (2008).
- Dunne, M., Corrigan, O. I. & Ramtoola, Z. Influence of particle size and dissolution conditions on the degradation properties of polylactide-co-glycolide particles. *Biomaterials* **21**, 1659–1668 (2000).
- Chen, H. *et al.* Hydrogel-thickened microemulsion for topical administration of drug molecule at an extremely low concentration. *Int. J. Pharm.* **341**, 78–84 (2007).
- Conchouso, D., Castro, D., Khan, S. A. & Foulds, I. G. Three-dimensional parallelization of microfluidic droplet generators for a litre per hour volume production of single emulsions. *Lab Chip* **14**, 3011–3020 (2014).
- Griffin, D. R. *et al.* Hybrid photopatterned enzymatic reaction (HyPER) for *in situ* cell manipulation. *ChemBioChem* **15**, 233–242 (2014).
- Schense, J. C. & Hubbell, J. A. Cross-linking exogenous bifunctional peptides into fibrin gels with factor XIIIa. *Bioconjug. Chem.* **10**, 75–81 (1999).
- Lutolf, M. P. & Hubbell, J. A. Synthetic biomaterials as instructive extracellular microenvironments for morphogenesis in tissue engineering. *Nature Biotechnol.* **23**, 47–55 (2005).
- Chen, E. J., Novakowski, J., Jenkins, W. K. & O'Brien, J. W. D. Young's modulus measurements of soft tissues with application to elasticity imaging. *IEEE Trans. Ultrason. Ferroelectr. Freq. Control* **43**, 191–194 (1996).
- Cheng, S. & Bilston, L. E. Unconfined compression of white matter. *J. Biomech.* **40**, 117–124 (2007).
- Parker, K. J., Huang, S. R., Musulin, R. A. & Lerner, R. M. Tissue response to mechanical vibrations for 'sonoelasticity imaging'. *Ultrasound Med. Biol.* **16**, 241–246 (1990).
- Samani, A., Bishop, J., Luginbuhl, C. & Plewes, D. B. Measuring the elastic modulus of *ex vivo* small tissue samples. *Phys. Med. Biol.* **48**, 2183–2198 (2003).
- Yeh, W.-C. *et al.* Elastic modulus measurements of human liver and correlation with pathology. *Ultrasound Med. Biol.* **28**, 467–474 (2002).
- Galiano, R. D., Michaels, J., Dobryansky, M., Levine, J. P. & Gurtner, G. C. Quantitative and reproducible murine model of excisional wound healing. *Wound Repair Regen.* **12**, 485–492 (2004).
- Fukano, Y. *et al.* Characterization of an *in vitro* model for evaluating the interface between skin and percutaneous biomaterials. *Wound Repair Regen.* **14**, 484–491 (2006).
- Fukano, Y. *et al.* Epidermal and dermal integration into sphere-templated porous poly(2-hydroxyethyl methacrylate) implants in mice. *J. Biomed. Mater. Res. A* **94A**, 1172–1186 (2010).
- Wang, H.-M. *et al.* Novel biodegradable porous scaffold applied to skin regeneration. *PLoS ONE* **8**, e56330 (2013).
- Wang, X., Ge, J., Tredget, E. E. & Wu, Y. The mouse excisional wound splinting model, including applications for stem cell transplantation. *Nature Protoc.* **8**, 302–309 (2013).
- Ota, T. *et al.* Notch signaling may be involved in the abnormal differentiation of epidermal keratinocytes in psoriasis. *Acta Histochem. Cytochem.* **47**, 175–183 (2014).
- Bramfeld, H., Sabra, G., Centis, V. & Vermette, P. Scaffold vascularization: A challenge for three-dimensional tissue engineering. *Curr. Med. Chem.* **17**, 3944–3967 (2010).
- Hollister, S. J. Porous scaffold design for tissue engineering. *Nature Mater.* **4**, 518–524 (2005).
- Yang, S., Leong, K.-F., Du, Z. & Chua, C.-K. The design of scaffolds for use in tissue engineering. Part I. Traditional factors. *Tissue Eng.* **7**, 679–689 (2001).
- Peters, M. C., Polverini, P. J. & Mooney, D. J. Engineering vascular networks in porous polymer matrices. *J. Biomed. Mater. Res.* **60**, 668–678 (2002).
- Winkler, E. A., Bell, R. D. & Zlokovic, B. V. Pericyte-specific expression of PDGF β receptor in mouse models with normal and deficient PDGF β receptor signaling. *Mol. Neurodegener.* **5**, 32 (2010).
- Huang, F.-J. *et al.* Pericyte deficiencies lead to aberrant tumor vascularization in the brain of the NG2 null mouse. *Dev. Biol.* **344**, 1035–1046 (2010).

47. Stratman, A. N., Malotte, K. M., Mahan, R. D., Davis, M. J. & Davis, G. E. Pericyte recruitment during vasculogenic tube assembly stimulates endothelial basement membrane matrix formation. *Blood* **114**, 5091–5101 (2009).
48. Rustad, K. C. *et al.* Enhancement of mesenchymal stem cell angiogenic capacity and stemness by a biomimetic hydrogel scaffold. *Biomaterials* **33**, 80–90 (2012).
49. Richardson, T. P., Peters, M. C., Ennett, A. B. & Mooney, D. J. Polymeric system for dual growth factor delivery. *Nature Biotechnol.* **19**, 1029–1034 (2001).
50. Sun, G. *et al.* Dextran hydrogel scaffolds enhance angiogenic responses and promote complete skin regeneration during burn wound healing. *Proc. Natl Acad. Sci. USA* **108**, 20976–20981 (2011).
51. Tokatlian, T., Cam, C. & Segura, T. Porous hyaluronic acid hydrogels for localized nonviral DNA delivery in a diabetic wound healing model. *Adv. Healthc. Mater.* <http://dx.doi.org/10.1002/adhm.201400783> (2015).
52. Liang, W. *et al.* Metabolically induced liver inflammation leads to NASH and differs from LPS- or IL-1 β -induced chronic inflammation. *Lab. Invest.* **94**, 491–502 (2014).
53. Latger-Cannard, V., Besson, I., Doco-Lecompte, T. & Lecompte, T. A standardized procedure for quantitation of CD11b on polymorphonuclear neutrophil by flow cytometry: Potential application in infectious diseases. *Clin. Lab. Haematol.* **26**, 177–186 (2004).
54. Lucas, T. *et al.* Differential roles of macrophages in diverse phases of skin repair. *J. Immunol.* **184**, 3964–3977 (2010).

Acknowledgements

The authors would like to thank A. Vucetic for assistance with gelation-kinetics measurements. This work was partially supported through the US National Institutes of Health Director's New Innovator Award (1DP2OD007113), NIH RO1HL110592, and the DermSTP Training Grant T32-AR058921.

Author contributions

D.R.G. and W.M.W. contributed equally to this manuscript, both in conceptual design, troubleshooting, experimental execution and manuscript writing. P.O.S. performed Day 1 immunological analysis and *in vivo* interpretation. D.D.C. and T.S. contributed equally to overseeing experimental design and interpretation.

Additional information

Supplementary information is available in the [online version of the paper](#). Reprints and permissions information is available online at www.nature.com/reprints.

Correspondence and requests for materials should be addressed to D.D.C. or T.S.

Competing financial interests

The authors have a financial interest in Tempo Therapeutics, which aims to commercialize MAP technology.